

Ge content optimization in Ge(SbSe)_1 − xN OTS materials for selector applications

Camille Laguna, Mathieu Bernard, Frederic Fillot, Denis Rouchon, Nevine Rochat, Julien Garrione, Lucie Prazakova, Emmanuel Nolot, Valentina Meli, Niccolo Castellani, et al.

▶ **To cite this version:**

Camille Laguna, Mathieu Bernard, Frederic Fillot, Denis Rouchon, Nevine Rochat, et al.. Ge content optimization in Ge(SbSe)_1 − xN OTS materials for selector applications. IEEE Transactions on Electron Devices, 2022, 69 (11), pp.6277-6283. 10.1109/TED.2022.3203368 . cea-03938734

HAL Id: cea-03938734

https://cea.hal.science/cea-03938734

Submitted on 13 Jan 2023

HAL is a multi-disciplinary open access archive for the deposit and dissemination of scientific research documents, whether they are published or not. The documents may come from teaching and research institutions in France or abroad, or from public or private research centers.

L'archive ouverte pluridisciplinaire **HAL**, est destinée au dépôt et à la diffusion de documents scientifiques de niveau recherche, publiés ou non, émanant des établissements d'enseignement et de recherche français ou étrangers, des laboratoires publics ou privés.

Ge Content Optimization in $Ge_X(SbSe)_{1-X}N$ OTS Materials for Selector Applications

C. Laguna, M. Bernard, F. Fillot, D. Rouchon, N. Rochat, J. Garrione,
L. Prazakova, E. Nolot, V. Meli, N. Castellani, S. Martin, C. Sabbione,
G. Bourgeois, M. C. Cyrille, L. Militaru, A. Souifi, F. Andrieu and G. Navarro

***Abstract*— In this paper, we investigate the influence of germanium content in GeSbSeN based Ovonic Threshold Selector (OTS) devices. We performed physico-chemical analyses on five different $Ge_x(SbSe)_{1-x}N$ alloys in order to understand how the germanium content influences the material structure and its integrity once submitted to temperatures up to 400°C. Thanks to electrical characterization of $Ge_x(SbSe)_{1-x}N$ OTS devices, we analyze the evolution of the electrical parameters along cycling up to 10^8 cycles and before and after annealing at 400°C. Cycle-to-cycle variability and drift phenomenon are also investigated. Finally, we demonstrate how Ge content should be properly tuned in order to improve the thermal stability of the alloy without affecting the leakage current and the electrical parameters variability.**

***Index Terms*— Ovonic Threshold Switching selector, GeSbSeN, Thermal stability, Electrical parameter variability.**

I. Introduction

OVONIC THRESHOLD SWITCHING (OTS) technology attracted a lot of attention from industry and motivated several research efforts in the last years for the possibility that it offers to fabricate ultra-highly dense Resistive Non-Volatile Memory Crossbar arrays with an agressive single memory cell area of $4F^2$. OTS is a key selector device that combines the capability to deliver a high current density when it is switched in the ON state, necessary for the programming of the memory element, and an ultra-low leakage current when it is in OFF state [1], [2]. Indeed, OTS and Phase-Change Memory (PCM) have been successfully co-integrated in a 3D-stackable 1S1R cell (i.e. one selector plus one resistive memory) [1], [3]–[5] and in recent years such device has achieved a level of reliability that allowed its commercialization in products targeting Storage Class Memory applications [6]. Several OTS amorphous chalcogenide alloys and dopants have been already investigated [1], [2], [7] and in recent years we have studied and demonstrated the intersting performances of GeSbSeN alloys (called "GSSN") to achieve low leakage current and high thermal stability [8], [9]. As we have previously reported, Ge-N bonds and Ge-Se bonds are fundamental to ensure the integrity of the amorphous nature of the OTS layer. In order to better highlight the role of Ge content in GeSbSeN system, we present in this work the study of $Ge_x(SbSe)_{1-x}N$ alloys featuring different Ge content. First, we investigate the layers as-deposited and after annealing at 400°C combining the results from Raman, FTIR spectroscopy and X-ray diffraction analysis (XRD). Therefore, thanks to the electrical characterization of integrated OTS devices, we compare the layers in terms of switching parameters and of their variability, thermal stability, endurance and drift along time of the threshold voltage. Finally, all these results are benchmarked showing the importance to correctly optimize the Ge content in GSSN alloy in order to achieve the best performances for selector applications.

This work was partially funded by European commission, French State and Auvergne-Rhône Alpes region through ECSEL-IA 101007321 project StorAIge and French Nano2022 program.
Camille Laguna, Mathieu Bernard, Frédéric Fillot, Denis Rouchon, Nevine Rochat, Julien Garrione, Lucie Prazakova, Emmanuel Nolot, Valentina Meli, Niccolò Castellani, Simon Martin, Chiara Sabbione, Guillaume Bourgeois, Marie Claire Cyrille, François Andrieu and Gabriele Navarro are with CEA, LETI, Univ. Grenoble Alpes, 38000 Grenoble, France.
Camille Laguna and Liviu Militaru are with Univ. de Lyon, INSA Lyon, ECL, CNRS, UCBL, CPE Lyon, INL, UMR 5270, INSA Lyon, 69621 Villeurbanne, France.
Abdelkader Souifi is with Univ. de Lyon, Ampere-UMR 5005, INSA Lyon, 69621 Villeurbanne, France.
Corresponding Author: Gabriele Navarro (gabriele.navarro@cea.fr)

II. Material characterization

We deposited our materials by magnetron reactive co-sputtering from Se-rich SbSe and Ge targets under constant N flow. We capped the samples for material analyses without air-break with 5 nm thick carbon layer in order to prevent the surficial oxidation. Germanium atomic ratio (x) in $Ge_x(SbSe)_{1-x}N$ was varied in the range 0.05 - 0.5, fabricating five different alloys addressed in the following as A, B, C, D and E: the material A is the poorer in Ge content while the material E is the richer. The annealing of the samples was performed applying an increasing temperature ramp (10 °C/min) up to the selected temperature.

In **Fig. 1**, we report the Raman spectra acquired on the as-deposited layers. The main feature, centered at 200 cm^{-1}, combines the bonds vibrations of both $SbSe_{3/2}$ pyramids (190 cm^{-1}) and $GeSe_{4/2}$ tetraedra connected by corners (200 cm^{-1}) and edges (214 cm^{-1}) [10]–[12] and is present in all the samples. The excess of Se in the system

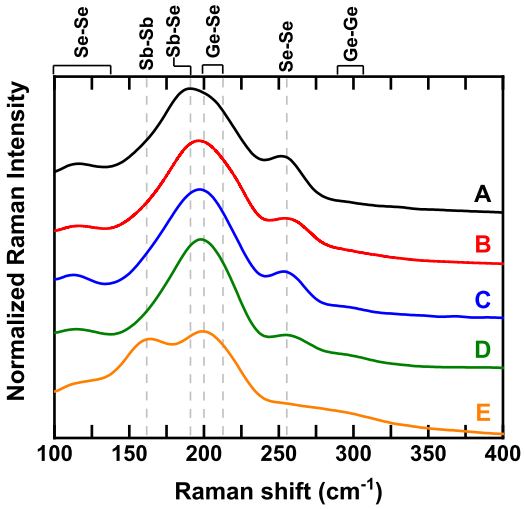


Fig. 1. Raman spectra of as-deposited materials. Main feature at 200 cm^{-1} is the result of the convolution of Sb-Se (at 190 cm^{-1}) and Ge-Se vibrations (at 200 and 210 cm^{-1}). Increasing Ge content from composition A to E, we observe a decrease of Se-Se mode (at 245-265 cm^{-1}) and an increase of Sb-Sb mode (at 160 cm^{-1}) [10]–[12].

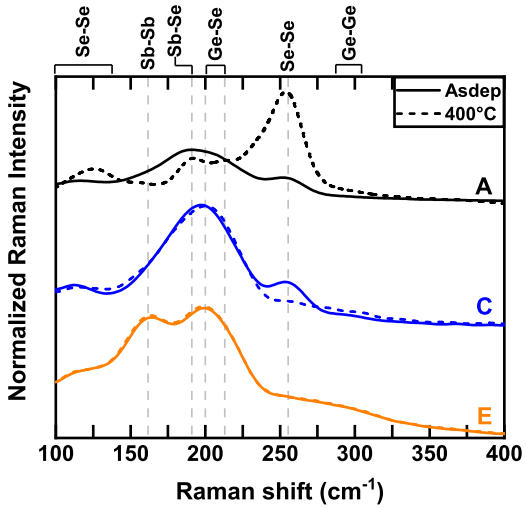


Fig. 2. Raman spectra for A, C and E samples as-deposited and after annealing at 400°C. Results from layers B and D are not reported for sake of clarity, being the results obtained for B close to A, and for D close to C. A strong Se segregation is observed in A leading to important material degradation. Annealing reduces Se segregation in C by slightly increasing the Ge-Se content. Material E stays stable after annealing.

gives rise to the formation of Se-Se weak homopolar bonds (bond energy = 44.04 kcal/mol [13]) that gradually decreases when increasing Ge content from A to E. We therefore observe the formation of stronger Ge-Se bonds (49.44 kcal/mol) with the reduction as well of the amount of Sb-Se features. Such impoverishment in Se of the Sb environment provides the gradual appearing of Sb-Sb vibrations, well visible in E. A high Ge content, like in E, is also responsible for the appearing of Ge-Ge modes (bond energy = 37.60 kcal/mol [14]–[16]) in the band from 250 cm^{-1} to 300 cm^{-1} [17]. A higher concentration of Ge-Se features at increasing Ge content should lead to an increase of the bandgap of the layer [10]. However, the appearing of Ge-Ge motifs at too much high Ge content, like in E composition, is expected to reduce the forbidden gap energy [13], [18], leading to a more conductive layer (i.e. higher leakage).

After the annealing at 400°C, we observe a reduction of the Ge-Se and Sb-Se feratures in A spectrum, with the increase in intensity of the Se homopolar feature (**Fig. 2**). This is likely correlated with Se phase segregation. A similar behavior has been observed in B layer (not reported). On the contrary in layer C (and D), the annealing leads to the disappearing of Se homopolar mode, as previously observed in [9], likely due to the layer reorganization in favor of stable Ge-Se features. Finally, almost no evolution is observed in sample E after 400°C annealing.

In **Fig. 3**, we report the FTIR spectra of as deposited materials. The spectra gather features linked to Sb-Se, Ge-Se and N-related bonds. Sb-Se feature at 201 cm^{-1} [19] does not present a significant correlation with respect to Ge content. The peak of Ge-Se feature (between 250 cm^{-1} and 300 cm^{-1}) is present in all the samples and it shifts towards lower frequencies incrasing Ge content. It means an increase of corner linked $GeSe_{4/2}$ tetrahedra (267 cm^{-1}) at the expense of edge linked $GeSe_{4/2}$ tetrahedra (294 cm^{-1}) [16], [19], [20] (due to higher Ge availability). The introduction of nitrogen in GeSbSe layers enables the formation of N-related bonds such as Sb-N, Ge-N and Se-N. The presence of modes between the positions of the known frequencies for such bonds [17], [21]–[24], are likely related to the presence of such bonds embedded in more complex features, nominally Sb-Se-N and Ge-Se-N. Such analysis is supported by the fact that Sb-Se-N features (indexed at about 640 cm^{-1}) well defined in A and B, decrease with the increasing of Ge content in C and D sample in favor of Ge-Se-N motifs (indexed at about 757 cm^{-1}). At even higher Ge content, Ge-N features (indexed at about 690 cm^{-1} [17], [23]) are promoted, together with Ge-Se-N ones still present in the system, in agreement with Raman results (Fig. 1).

After annealing at 400°C, the shift of Sb-Se and Ge-Se features towards lower frequencies in sample A (**Fig. 4**) are the indication of an advanced evolution (i.e. degradation) of the layer integrity. This is in line with Raman analysis (Fig. 2) and likely due to the starting of Se segregation. Moving to higher Ge contents, after annealing, Ge-N features are favoured (Ge-N and Ge-Se-N) with the narrowing and the intensity increase of the motif between 700 cm^{-1} and 800 cm^{-1}.

From XRD analysis performed on all the sample after the annealing at 400°C, we observe that only material E remains completely amorphous **Fig. 5**. In the other samples, Sb_2Se_3 crystallites appear with increasing peaks intensity moving towards $Ge_x(SbSe)_{1-x}N$ alloys with lower Ge content. We think that the higher concentration of Ge-N and Ge-Se-N features at increasing Ge content, allows retarding the crystallization phenomena, similarly to what already observed in other chalcogenide layers [17].

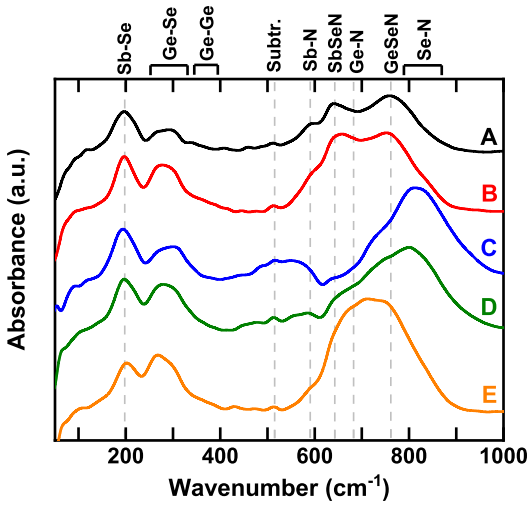


Fig. 3. FTIR spectra of as-deposited materials. Main features are identified to be related to Sb-Se at 201 cm^{-1} [19], Ge-Se at 250-300 cm^{-1} [16], [19], [20] and N-related bonds above 590 cm^{-1} [17], [21]–[24].

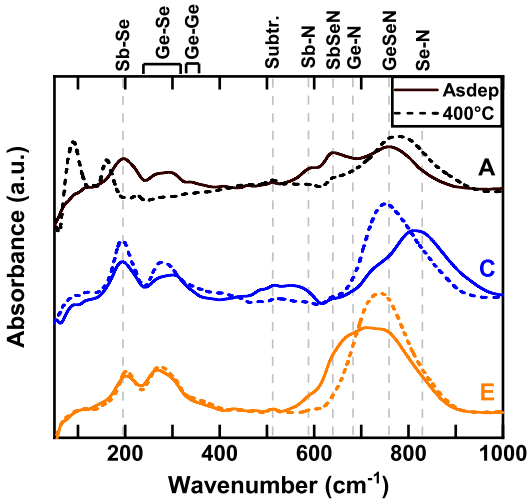


Fig. 4. FTIR spectra for A, C and E samples as-deposited and annealed at 400°C. A material is degraded by the 400°C annealing, as show the Sb-Se and Ge-Se features. Considering the N-related bonds, annealing tends to reduce the number of different features favouring stable Ge-N or Ge-Se-N bonds [23].

Increasing Ge content in $Ge_x(SbSe)_{1-x}N$ system we increase the amount of Ge-Se and Ge-N bonds, respectively responsible for a higher bandgap, important to reduce the OTS device leakage, and a higher thermal stability up to 400°C. However, too high Ge content could lead to the formation of Ge-Ge features, likely responsible for a higher conductivity (i.e. higher leakage).

III. Electrical Characterization

We integrated $Ge_x(SbSe)_{1-x}N$ layers in analytical OTS devices as described in **Fig. 6**. A thin carbon layer between titanium nitride top electrode and chalcogenide layer prevents Ti diffusion in the chalcogenide layer either during fabrication or device operation [25]. All

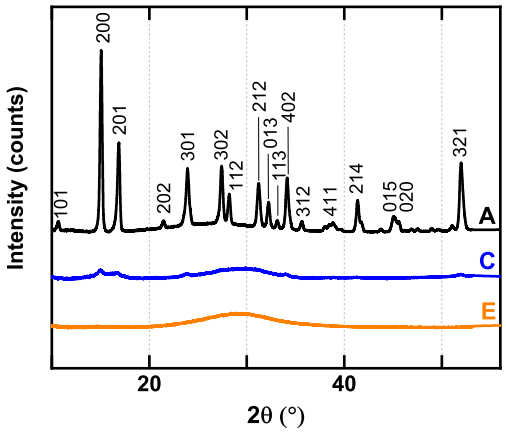


Fig. 5. XRD spectra for materials A to E annealed at 400°C. B and D spectra match A and C spectra respectively (not reported). E material remains perfectly amorphous after annealing (i.e. no crystalline patterns). Peaks detected in the other samples are attributed to Sb_2Se_3 crystalline phase (orthorhombic Pnma (62) space group of ICDD database).

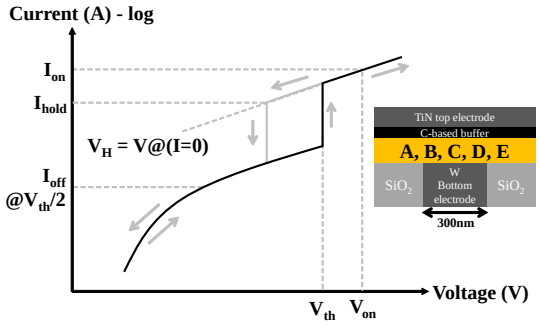


Fig. 6. Schematic IV curve for an OTS device and main electrical parameters: V_{th} is the threshold voltage; V_H is the holding voltage; I_{on} is the current measured during the programming operation (V_{on}); I_{hold} is the minimum current to preserve the OTS in the ON regime; I_{off} is the leakage current measured at $V_{th}/2$. The inset presents the OTS device integrating $Ge_x(SbSe)_{1-x}N$ layers (A to E) deposited over a tungsten based bottom electrode with a diameter of about 300 nm.

the results are collected from populations of about ten devices. Main electrical parameters reported in the following are defined in Fig. 6 and collected by AC measurements (i.e. pulsed voltages/currents).

A. Electrical parameters

We compared the electrical parameters of $Ge_x(SbSe)_{1-x}N$ OTS devices before and after an annealing of 30 minutes at 400°C.

By increasing Ge content in as-fabricated devices from composion A to D, and thus increasing the GeSe content as observed in previous section, we increase the material gap and its resistivity, which lead to a higher fire voltage (V_{fire} i.e. the initialization voltage), a higher threshold voltage (V_{th}) (**Fig. 7**) and a reduced leakage current I_{off} (**Fig. 8**). This trend is inversed in E composition, where the presence of Ge-Ge features decreases the bandgap [13], [18] and thus the switching voltages, combined to an increase of I_{off}. Holding parameters, V_H (holding voltage) and I_{hold} (holding current), do not show a

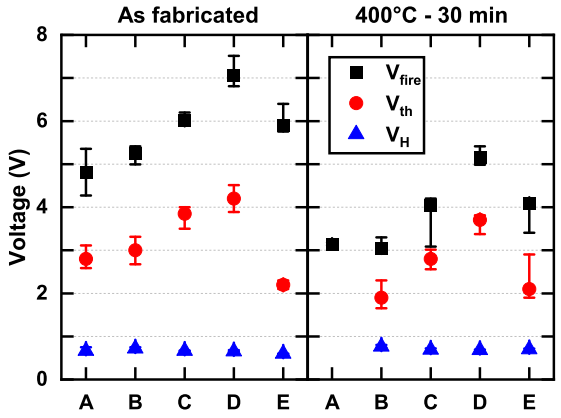


Fig. 7. V_{fire}, V_{th}, V_H measured for all $Ge_x(SbSe)_{1-x}N$ OTS devices before and after annealing at 400°C. The values of V_{th} and V_H are collected after 1000 cycles (to confirm the device reliable functionality and stable cycle-to-cycle parameters).

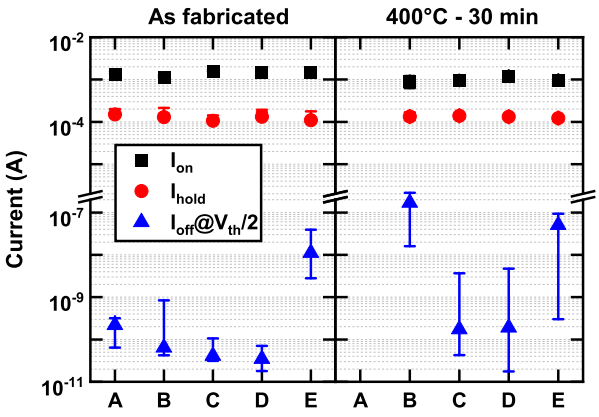


Fig. 8. I_{on}, I_{hold} and I_{off} measured for the $Ge_x(SbSe)_{1-x}N$ OTS devices before and after annealing at 400°C. The parameters are acquired after 1000 cycles. Data for material A are not reported after annealing due to devices failure related to the layer crystallization (Fig. 5).

dependency on Ge content, likely due to the equivalent nature of the ON state in the five different alloys. Indeed, SbSe system is present in all the studied layers, more or less prevented from crystallization (Fig. 5).

The previous observations are still valid after the annealing at 400°C, that mainly causes a reduction of V_{fire} and V_{th}, and an increase of I_{off} which still remains in the nA range for C and D compositions. The starting of SbSe crystallzation (Fig. 5) and the structural relaxation [9] are the main responsibles for such evolution. Material A is not anymore functional after annealing, due to the segregation (Fig. 2) and crystallization of Sb_2Se_3 that features a crystallization temperature equal to 217°C [26] (Fig. 5).

The summary of the observed evolution after annealing of I_{off} and V_{th} is reported in **Fig. 9**. As expected, independently from the evolution of each material caused by the annealing, a decrease of V_{th} (i.e. lower bandgap of the material) is linked to an increase of I_{off} (i.e. higher conductivity). Moreover, as reported in the inset, the higher the Ge content, the lower the V_{th} and I_{off} variation before and after annealing. This behavior matches the

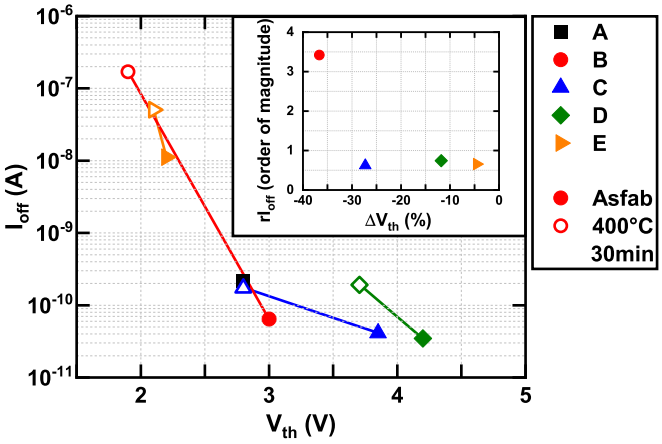


Fig. 9. I_{off} as a function of V_{th} for $Ge_x(SbSe)_{1-x}N$ devices, extracted from Fig. 7 and Fig. 8, before and after annealing. Inset: variation of the order of magnitude of I_{off} (rI_{off}), calculated as the $\log_{10}$ of the ratio between the value after and before annealing, as a function of the V_{th} variation in % before and after annealing.

physico-chemical results presented in Fig. 2 and Fig. 4, in which high Ge content leads to almost unchanged spectra after annealing at 400°C (i.e. higher thermal stability induced by Ge-N and Ge-Se-N features).

B. Subthreshold conduction analysis

Fig. 10 reports median I-V characteristics after 10 cycles for as fabricated $Ge_x(SbSe)_{1-x}N$ devices. Experimental data are in agreement with Poole-Frenkel conduction. The intertrap distance and activation energy E_a [27] are extracted from to the following relations

$$STS = \frac{\partial \ln(I)}{\partial V} = \frac{q}{kT}\frac{\Delta z}{2u_a} \quad (1)$$

$$\ln(I/V) \propto \frac{E_a + \beta_{PF} V^{1/2}}{kT} \quad (2)$$

where STS is the subthreshold slope, k the Boltzmann constant, T the room temperature (25°C), Δz the intertrap distance, u_a the layer thickness and β_{PF} a coefficient.

The observed trend for Δz and E_a is in agreement with the observed trends for the electrical parameters (i.e. V_{th}, I_{off}). Indeed, for material A the gap is reduced by the likely formation of SbSe features, and in material E by the segregation of Ge. For intermediate Ge contents (B, C, D) the amorphous nature of the layer is on the contrary preserved.

C. Endurance and cycle-to-cycle variability

We studied the impact of cycling on as-fabricated $Ge_x(SbSe)_{1-x}N$ OTS devices. We studied the endurance up to 10^8 and the cycle-to-cycle variability evaluated after 10^4 cycles.

In **Fig. 11** we report the variation of I_{off} as a function of the variation V_{th} during cycling, along with the evolution of the absolute values of I_{on} and I_{off} (in the

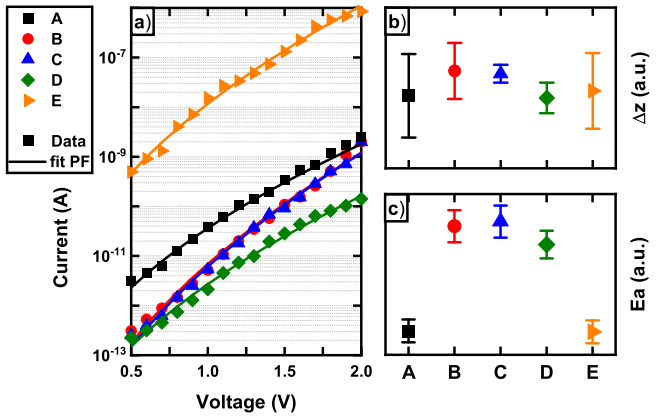


Fig. 10. **a)** Median I-V characteristics with Poole-Frenkel fits, **b)** Intertrap distance calculated with eq. (1) and, **c** Activation energy E_a extracpolated from eq. (2).

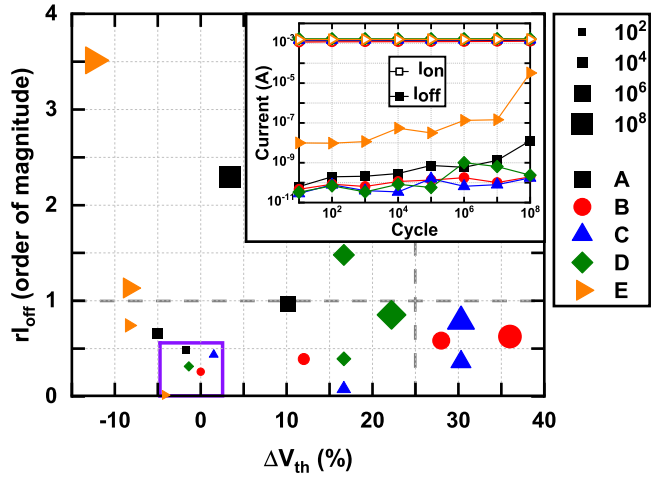


Fig. 11. Endurance results for $Ge_x(SbSe)_{1-x}N$ OTS devices. I_{off} variation along cycling (in orders of magnitude) is reported as a function of the variation of V_{th} in %. The data are reported from 10^2 up to 10^8 cycles with increasing symbols size. The dotted lines highlight the region (at the bottom-left of the graph) in which it would suitable to maintain the variation of both I_{off} and V_{th} along cycling. The square at the bottom evidences the region of the graph in which all the five material start at the beginning of the cycling (i.e. after only 10^2 cycles). Inset: evolution along cycles of I_{on} and I_{off} for the five materials.

inset). Materials A, B, C and D reach 10^8 cycles keeping a selectivity of at least 10^5 (i.e. ratio between I_{on} and I_{off}). Material E on the contrary shows an increasing leakage along cycling. I_{off} variation (rI_{off}) and V_{th} variation (ΔV_{th}) are calculated as follows:

$$rI_{off} = \log_{10}\left(\frac{I_{off}(N)}{I_{off}(1)}\right) \quad (3)$$

$$\Delta V_{th} = \frac{V_{th}(N) - V_{th}(1)}{V_{th}(1)} \quad (4)$$

where $I_{off}(N)$ and $V_{th}(N)$ are respectively the I_{off} and the V_{th} measured at cycle N. Material A presents a good compromise in terms of I_{off} increase (only about 2 orders of magnitude) with an extremely low V_{th} variation along cycling. A low V_{fire}, as reported in Fig. 7, avoids a too high stress of the material at the initialization step, and this should maintain the switching properties of

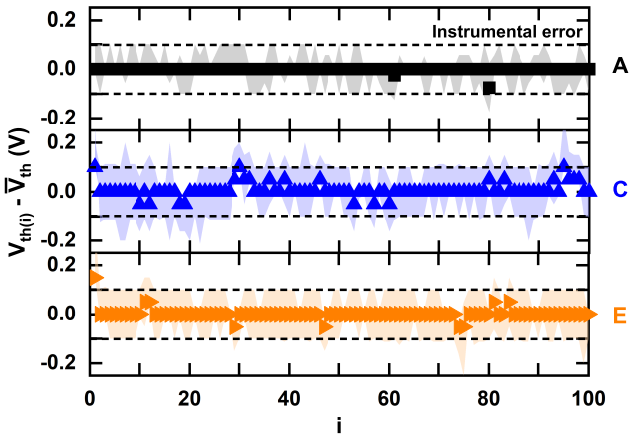


Fig. 12. V_{th} cycle-to-cycle variation measured along 100 switching operations, after 10^4 cycles. The V_{th} variation (y-axis) is calculated as the difference between V_{th} measured at i-th cycle ($V_{th}(i)$) and the mean value of V_{th} calculated for the 100 consecutive cycles ($\overline{V_{th}}$).

the SbSe system (i.e. main system present in material A as observable in spectra of Fig. 1 and Fig. 3) without triggering the crystallization within 10^8 cycles.

Despite a low I_{off} evolution along cycling, materials B, C and D show a considerable evolution of V_{th}, with a minimum for material D that presents a V_{th} variation of less than 25%. Similarly to what observed after annealing, an intermediate Ge content is responsible for more Ge-N and Ge-Se-N features that help in maintaining the amorphous nature of the layer (i.e. low leakage) but with an increase in the stability of such features at high temperature (i.e. FTIR results in Fig. 4), and a consequent increase of the bandgap and of the V_{th} of the material along cycling.

Finally, material E shows the inversion of the trend with a reduction of V_{th} along cycling together with the increase of I_{off}, likely due to the ongoing Ge segregation attributable to the presence of Ge-Ge features already in the as-deposited layer Fig. 1. In this case, despite an observed high stability and delayed crystallization at high temperature, the rising of the temperature well above 400°C during programming operations should be responsible for Ge segregation, similarly to what previously observed in other Ge-rich chalcogenides [17]. Ge crystallization then induces a decrease of the bandgap of the material and a higher leakage.

In **Fig. 12**, we present the V_{th} cycle-to-cycle variation after 10^4 cycles. V_{th} value was measured 100 times consecutively with a V_{th} sensitivity of 0.1 V. No major differences are observed between materials and devices, with a really high stability of V_{th} in the range of cycles explored. The differences should be found only for high cycles number, as reported in Fig. 11.

D. Threshold voltage drift

Fig. 13 reports the evolution of V_{th} along time for all the $Ge_x(SbSe)_{1-x}N$ devices. V_{th} drift follows the follow-

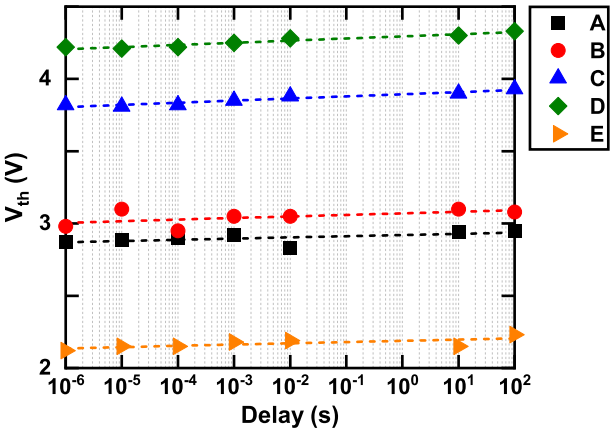


Fig. 13. V_{th} measured after 1 μs, 10 μs, 100 μs,1 ms, 10 ms, 10 s and 100 s delay. Dashed lines represent the fitting curves obtained using equation eq. (5).

ing empirical rule:

$$V_{th}(t) = \alpha \ln\left(\frac{t}{t_0}\right) + V_{th}(t_0) \quad (5)$$

where α is the drift coefficient and $V_{th}(t_0)$ is the value of V_{th} at time equal to t_0 (in our case 1 μs). We observe an ultra low drift within the studied delays **Fig. 14**. Vth drift is more important for materials with high threshold voltage like C and D. The higher Ge content of these layers (with respect to A and B) likely leads to the formation of Ge-Ge bonds and Ge-Sb wrong bonds after the melt-quench process following the pulse application. However, the presence of stable Ge-Se units hinders the crystallization of the material during the pulse application, leaving the system in a disordered and amorphous phase (i.e. with a high bandgap and resistivity). As reported in [28], the structural relaxation in amorphous systems implies the suppression of homopolar or wrong bonds along time (like in C and D), if they are not leading to the formation of stable nuclei of a segregated phase. On the contrary, materials A and B feature a higher SbSe content with less probability to form Ge-Ge homopolar bonds and the possibility on the contrary to form stable heteropolar bonds proper to SbSe crystalline phase (Fig. 5). Materials with higher drift are the ones with higher activation energy as reported in Fig. 10. These observations could be put in parallel with the work of [29] which reports that numerous Ge-Ge bonds lead to more slow defects that remain delocalized after device turn OFF along endurance study, causing degradation. To conclude, as already highlighted during cycling, material E is featuring Ge segregation and crystallization since first cycles. The increase of the conductivity due to formation of percolation paths in the material, leads to a lower sensitivity to the relaxation phenomena happening in the units owning to the still amorphous volume of the layer.

The electrical characterization of $Ge_x(SbSe)_{1-x}N$ OTS devices showed that thermal stability is improved increasing the Ge content up to a maximum value (composition D), after which the layer likely undergoes the segregation phenomenon (composition E). Endurance up to 10^8 is achievable in all the samples with some compromises: too low Ge content could lead to early SbSe crystallization with an increase of I_{off}, too high Ge content could lead to a fast degradation of switching properties still due to Ge segregation. At intermediate Ge contents, an optimum should be found (composition D) to avoid a too high V_{th} variation during cycling due to enhanced Ge-/N-related features (Ge-Se-N and Ge-N). Finally, the drift of V_{th} is correlated as well with previous observations, in particular revealing the possible impact of Ge-Ge homopolar bonds relaxation in Ge-rich amorphous layers with intermediate Ge content (compositions C and D).

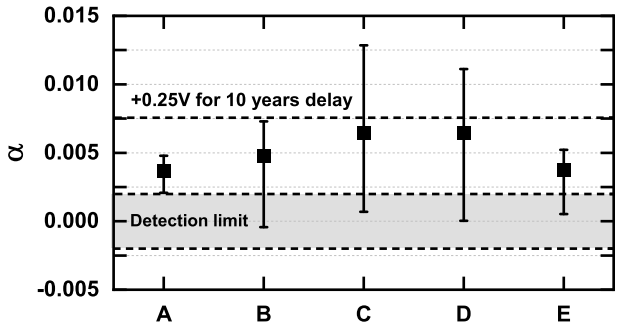


Fig. 14. Drift coefficient α measured thanks to eq. (5). We can observe that C and D materials present the highest drift, leading to an increase of 0.25 V (i.e. about + 6%) after 10 years. Some devices present an α value too low to be measured correctly (grey banner, under detection limit).

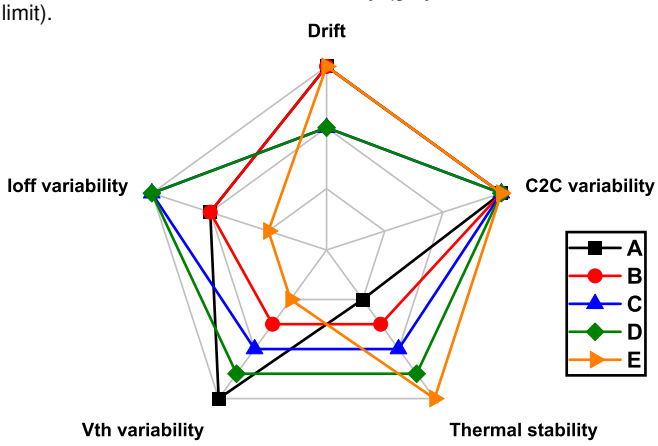


Fig. 15. Radar graph showing the different electrical performances studied in $Ge_x(SbSe)_{1-x}N$ OTS devices. Best compromise should be found in layers with intermediate Ge content i.e. C and D compositions.

IV. Conclusions

In this paper, we have investigated the influence of Ge content in Se-rich $Ge_x(SbSe)_{1-x}N$ alloys through material and electrical analyses. We have demonstrated that increasing Ge content improves the thermal stability at 400°C, with an optimum for intermediate Ge contents. The proper tuning of Ge content, allows the best compromise in terms of I_{off} and V_{th} variation along cycling, with

an endurance up to more than 10^8 cycles, still ensuring low V_{th} drift in time (**Fig. 15**).

REFERENCES

[1] H. Y. Cheng, W. C. Chien, I. T. Kuo, C. W. Yeh, L. Gignac, W. Kim, E. K. Lai, Y. F. Lin, R. L. Bruce, C. Lavoie, C. Cheng, A. Ray, F. M. Lee, F. Carta, C. H. Yang, M. H. Lee, H. Y. Ho, M. BrightSky, and H. L. Lung, "Ultra-High Endurance and Low IOFF Selector based on AsSeGe Chalcogenides for Wide Memory Window 3D Stackable Crosspoint Memory," in *2018 IEEE International Electron Devices Meeting (IEDM)*. IEEE, 2018, pp. 37.3.1–37.3.4.

[2] D. Garbin, W. Devulder, R. Degraeve, G. L. Donadio, S. Clima, K. Opsomer, A. Fantini, D. Cellier, W. G. Kim, M. Pakala, A. Cockburn, C. Detavernier, R. Delhougne, L. Goux, and G. S. Kar, "Composition Optimization and Device Understanding of Si-Ge-As-Te Ovonic Threshold Switch Selector with Excellent Endurance," in *2019 IEEE International Electron Devices Meeting (IEDM)*. IEEE, 2019, pp. 35.1.1–35.1.4.

[3] D. C. Kau, "The pursuit of atomistic switching and cross point memory," in *2021 International Symposium on VLSI Technology, Systems and Applications (VLSI-TSA)*, 2021, pp. 1–2.

[4] W. Chien, L. Gignac, N. Gong, C. Yeh, C. Yang, R. Bruce, H. Cheng, J. Papalia, H. Miyazoe, C. Cheng, W. Kim, I. Kuo, F. Carta, A. Ray, E. Lai, M. BrightSky, and H. Lung, "Solution for PCM and OTS Intermixing on Cross-Point Phase Change Memory," in *2019 IEEE 11th International Memory Workshop (IMW)*. IEEE, 2019, pp. 1–4.

[5] G. Navarro, A. Verdy, N. Castellani, G. Bourgeois, V. Sousa, G. Molas, M. Bernard, C. Sabbione, P. Noé, J. Garrione, L. Fellouh, and L. Perniola, "Innovative PCM+OTS device with high subthreshold non-linearity for non-switching reading operations and higher endurance performance," in *2017 Symposium on VLSI Technology*, 2017, pp. T94–T95.

[6] H.-Y. Cheng, F. Carta, W.-C. Chien, H.-L. Lung, and M. J. BrightSky, "3D cross-point phase-change memory for storage-class memory," *Journal of Physics D: Applied Physics*, vol. 52, no. 47, p. 473002, sep 2019.

[7] N. S. Avasarala, B. Govoreanu, K. Opsomer, W. Devulder, S. Clima, C. Detavernier, M. van der Veen, J. Van Houdt, M. Henys, L. Goux, and G. S. Kar, "Doped GeSe materials for selector applications," in *2017 47th European Solid-State Device Research Conference (ESSDERC)*, 2017, pp. 168–171.

[8] A. Verdy, G. Navarro, V. Sousa, P. Noe, M. Bernard, F. Fillot, G. Bourgeois, J. Garrione, and L. Perniola, "Improved Electrical Performance Thanks to Sb and N Doping in Se-Rich GeSe-Based OTS Selector Devices," in *2017 IEEE International Memory Workshop (IMW)*, 2017, pp. 1–4.

[9] A. Verdy, M. Bernard, J. Garrione, G. Bourgeois, M. C. Cyrille, E. Nolot, N. Castellani, P. Noé, C. Socquet-Clerc, T. Magis, G. Sassine, G. Molas, G. Navarro, and E. Nowak, "Optimized Reading Window for Crossbar Arrays Thanks to Ge-Se-Sb-N-based OTS Selectors," in *2018 IEEE International Electron Devices Meeting (IEDM)*, 2018, pp. 37.4.1–37.4.4.

[10] M. Olivier, J. Tchahame, P. Nemec, M. Chauvet, V. Besse, C. Cassagne, G. Boudebs, G. Revversez, R. Boidin, E. Baudet, and V. Nazabal, "Structure, nonlinear properties, and photosentisivity of $GeSe_2$(100-x)Sb_2Se_3(x) glasses," *Optical Materials Express*, vol. 4, no. 3, pp. 525–540, 2014.

[11] K. Jackson, A. Briley, S. Grossman, D. V. Porezag, and M. R. Pederson, "Raman-active modes of a-$GeSe_2$ and a-GeS_2 : A first-principles study," *Physical Review B*, vol. 60, no. 22, pp. R14 985–R14 989, 1999.

[12] E. Baudet, C. Cardinaud, A. Girard, E. Rinnert, K. Michel, B. Bureau, and V. Nazabal, "Structural analysis of RF sputtered Ge-Sb-Se thin films by Raman and X-ray photoelectron spectroscopies," vol. 444, pp. 64–72, 2016.

[13] N. Sharma, S. Sharda, V. Sharma, and P. Sharma, "Far-infrared investigation of ternary Ge–Se–Sb and quaternary Ge–Se–Sb–Te chalcogenide glasses," *Journal of Non-Crystalline Solids*, vol. 375, pp. 114–118, 2013.

[14] S. A. Saleh, "Synthesis and Characterization of $Sb_{65}Se_{35-x}Ge_x$ Alloys," *Materials Sciences and Applications*, vol. 2, no. 7, pp. 950–956, 2011.

[15] J. H. Lee, W. H. Lee, J. K. Park, J. H. Yi, S. Y. Shin, B. J. Park, B. So, J. Heo, J. H. Choi, H. J. Kim, and Y. G. Choi, "Thermal properties of ternary Ge–Sb–Se chalcogenide glass for use in molded lens applications," *Journal of Non-Crystalline Solids*, vol. 431, pp. 41–46, 2016.

[16] S. Sharda, N. Sharma, P. Sharma, and V. Sharma, "Finger prints of chemical bonds in Sb–Se–Ge and Sb–Se–Ge–In glasses: A Far-IR study," *Journal of Non-Crystalline Solids*, vol. 362, pp. 136–139, 2013.

[17] L. Prazakova, E. Nolot, E. Martinez, F. Fillot, D. Rouchon, N. Rochat, M. Bernard, C. Sabbione, D. Morel, N. Bernier, A. Grenier, A. Papon, M. Cyrille, and G. Navarro, "Temperature driven structural evolution of Ge-rich GeSbTe alloys and role of N-doping," *Journal of Applied Physics*, vol. 128, no. 21, p. 215102, 2020.

[18] G. Saffarini, J. M. Saiter, and H. Schmitt, "The composition dependence of the optical band gap in Ge–Se–In thin films," *Optical Materials*, vol. 29, no. 9, pp. 1143–1147, 2007.

[19] D. R. Goyal and A. S. Maan, "Far-infrared absorption in amorphous $Sb_{15}Ge_xSe_{85-x}$ glasses," *Journal of Non-Crystalline Solids*, vol. 183, no. 1, pp. 182–185, 1995.

[20] P. K. Dwivedi, S. K. Tripathi, A. Pradhan, V. N. Kulkarni, and S. C. Agarwal, "Raman study of ion irradiated GeSe films," *Journal of Non-Crystalline Solids*, vol. 266-269, pp. 924–928, 2000.

[21] J. Buckeridge, D. Scanlon, T. Veal, M. Ashwin, A. Walsh, and R. Catlow, "N incorporation and associated localized vibrational modes in GaSb," *Phys. Rev. B*, vol. 89, p. 014107, 01 2014.

[22] T. Shiraishi, Y. Arai, and S. Yamazaki, "Optical and electrical properties on transparency a-SbN films," *Journal of Non-Crystalline Solids*, vol. 77-78, pp. 1313–1316, 1985, proceedings of the Eleventh International Conference on Amorphous and Liquid Semiconductors.

[23] I. Chambouleyron and A. R. Zanatta, "Nitrogen in germanium," *Journal of Applied Physics*, vol. 84, no. 1, pp. 1–30, 1998.

[24] L. Andrews, P. Hassanzadeh, D. V. Lanzisera, and G. D. Brabson, "Reactions of Selenium in a Quartz Discharge Tube. Infrared Spectra and Density Functional Theory Calculations of New Selenium Nitrogen and Selenium Silicon Species in Solid Argon," *The Journal of Physical Chemistry*, vol. 100, no. 41, pp. 16 667–16 673, Jan. 1996.

[25] A. Verdy, G. Navarro, M. Bernard, S. Chevalliez, N. Castellani, E. Nolot, J. Garrione, P. Noe, G. Bourgeois, V. Sousa, M.-C. Cyrille, and E. Nowak, "Carbon electrode for Ge-Se-Sb based OTS selector for ultra low leakage current and outstanding endurance," in *2018 IEEE International Reliability Physics Symposium (IRPS)*. Burlingame, CA: IEEE, Mar. 2018, pp. 6D.4–1–6D.4–6.

[26] S. Bordas, M. Clavaguera-Mora, and B. Legendre, "Phase diagram of the ternary system Ge-Sb-Se," *Thermochimica Acta*, vol. 56, no. 2, pp. 161–182, 1982.

[27] D. Ielmini and Y. Zhang, "Analytical model for subthreshold conduction and threshold switching in chalcogenide-based memory devices," *Journal of Applied Physics*, vol. 102, no. 5, p. 054517, Sep. 2007.

[28] W. Zhang and E. Ma, "Unveiling the structural origin to control resistance drift in phase-change memory materials," *Materials Today*, vol. 41, pp. 156–176, 2020.

[29] F. Hatem, Z. Chai, W. Zhang, A. Fantini, R. Degraeve, S. Clima, D. Garbin, J. Robertson, Y. Guo, J. F. Zhang, J. Marsland, P. Freitas, L. Goux, and G. S. Kar, "Endurance improvement of more than five orders in Ge_xSe_{1-x} OTS selectors by using a novel refreshing program scheme," in *2019 IEEE International Electron Devices Meeting (IEDM)*, 2019, pp. 35.2.1–35.2.4.